



Sharif University of Technology

Scientia Iranica

*Transactions A: Civil Engineering*

<http://scientiaranica.sharif.edu>



# Probabilistic collapse assessment of steel frame structures considering the effects of soil-structure interaction and height

M. Sabouniaghdam, E. Mohammadi Dehcheshmeh, P. Safari, and V. Broujerdi\*

School of Civil Engineering, Iran University of Science and Technology, Tehran, P.O. Box 16765-163, Iran.

Received 13 July 2021; received in revised form 26 December 2021; accepted 22 February 2022

## KEYWORDS

Exceedance probability;  
Fragility curve;  
Incremental dynamic analysis;  
Performance level;  
Intermediate moment-resisting steel frame;  
Soil-structure interaction.

**Abstract.** This paper investigates the seismic performance of intermediate moment-resisting steel frame structures considering the effects of height and soil-structure interaction. For this purpose, three 3D structures of 3-, 6-, and 9-story buildings were designed using CSI ETABS software in accordance with ASCE7-16. Then, the 2D frames of the structures were simulated by OpenSees software and to account for the nonlinearity of the material, the plastic hinge elements were used. The 2D frames were analyzed using Incremental Dynamic Analysis (IDA) method subjected to 22 far-field ground motion records of FEMA-P695. Finally, the fragility curves of the structures were developed. The results illustrated that consideration of soil-structure interaction led to lower spectral acceleration as height increased, meaning that higher-rising structures had record-induced  $S_a(T_{1,5\%})$  closer to  $S_a(\text{Design})$  and upon decreasing height, the difference tended to increase. Exceedance probability decreased with increase in the structure's height, and consideration of the soil-structure interaction adapts to lower exceedance probability. Moreover, the investigated intermediate moment-resisting steel frame structural models designed according to ASCE7-16 consideration exhibited acceptable seismic performance against far-field records. Their exceedance probabilities in terms of Life Safety (LS) and Collapse Prevention (CP) performance levels are less than 0.45 and 0.03, respectively.

© 2022 Sharif University of Technology. All rights reserved.

## 1. Introduction

### 1.1. Background

Nowadays, with the widespread application of performance-based design approach, considering the effects of soil-structure interaction has become clearer than before. New generation of performance-based standard codes emphasizes considering all the factors

affecting the seismic performance of structures, in particular soil-structure interaction [1].

Due to uncertainties in performance assessment of structures, probabilistic formulation is used for such investigations. Thanks to the advancement of structural assessment by performance levels and its ability to predict structural collapse, it is possible to connect the affecting performance factors to the performance level of structures and then, to carry out the structural assessment based on performance levels. The soil-structure interaction is one of the factors involved in causing many earthquake-induced structural damages. Lessons learned from previous earthquakes highlight the necessity of applying soil-structure interaction to

\*. Corresponding author. Tel.: +98 21 77240399;  
Fax: +98 21 77240398  
E-mail address: broujerdi@iust.ac.ir (V. Broujerdi)

the design and analysis of structures. For instance, the majority of structural collapses and damages of the Loma Prieta earthquake in 1989 are found to be caused by this vital, yet complicated, phenomenon [2].

For many years, it has been the sole objective of seismic codes to design structures with high levels of structural resistance against earthquakes. Ductile design of structures happens to be the prime solution achieving such an aim. Amongst structural systems, moment-resisting steel frames produce high levels of ductility. Moment-resisting connections directly affect the ductile behavior of such frames. Observed damages to moment-resisting steel connections caused by the earthquakes of Northridge in 1994 and Kobe in 1995 forced researches to investigate extensively the seismic behavior of moment-resisting steel frames and their connections. This system is categorized into 3 types of ordinary, intermediate, and special moment-resisting frames indicating different seismic behaviors [3].

It is a complex process to predict the seismic performance of structures against the future earthquakes. Performance-based design is a new method employed by most of standard codes and manuals such as ATC-40, SAC/FEMA350 [3], and FEMA356 [4]. Normally, such codes attempt to design a specific structure for a set of performance-based objectives and against a probable future earthquake within its service life. For instance, a building structure with a service life of 50 years can be designed so as not to receive any damage from earthquakes with 50% occurrence probability within 50 years, but it will receive acceptable structural and non-structural damages from earthquakes with 10% occurrence probability within 50 years. In addition, for earthquakes with 2% occurrence probability in 50 years, the structure will inevitably face serious damages which should withstand without collapse.

Therefore, development of methods for structural demand estimation in order to determine direct and indirect damages is highly important. Until now, various methods of seismic demand estimation have been introduced, but the Incremental Dynamic Analysis (IDA) method has been accepted and extensively used by researches in academia [5].

In the method of IDA, a structure will be analyzed under a specific set of selected earthquake records at different levels of seismic intensity (all the records will be scaled); thus, seismic behavior of the structure will be determined completely against all the seismic intensities. Using fragility curves resulting from uniformed IDA curves (16%, 50%, 84%), corresponding capacity of collapse, and performance levels mixed with the earthquake's hazard properties, the yearly demand of occurrence probability can be calculated. For this purpose, the application of fragility curves which present the conditional probability and exceed the

probability from a pre-defined damage level has gained a tremendous popularity amongst research scientists.

## 1.2. Literature review

The first study conducted on the subject of soil-structure interaction dates back to the year 1932 [6] when earthquake-induced structural damage of buildings constructed on different types of soil was investigated. Later on in the 1930s, with the theory of wave propagation, seismic vibration mitigation of structures using energy dissipation within soil was studied which for 50 years directed the researchers to state that major vibrational damping of structures occurs at the interface of the foundation with ground [7]. Effect of soil rigidity on the structural responses using numerical methods was studied too [8]. In 1956, the complexity of analyzing soil-structure interaction due to lack of knowledge on the wave propagation phenomenon in soil layers of having ultra-inhomogeneity nature was clearly stated [9]; however, gradually, it was perceived that considering soil-structure interaction led to recording more realistic structural behaviors [10]. Furthermore, the effects of foundation pull-up and soil yielding were studied based on experimental tests [11]. In the latest conducted researches, a study investigated the behavior of asymmetric sliding buildings with steel moment frame systems subject to earthquake loading (both horizontal and vertical) while taking into account the effects of soil-structure interaction [12]. A six-story steel frame model considering soil-structure interaction was tested by shake table test and numerically simulated to investigate the effects of different soil types, structural properties, and soil-structure interaction which showed that soil-structure interaction effects could noticeably mitigate the dynamic response of structures [13]. Seismic response of mid-rise steel moment-resisting frames considering the role of geometrical irregularity, frequency components of near-fault records, and soil-structure interaction was investigated to indicate the important role of residual frequency component and soil-structure interaction [14]. A novel probabilistic approach to considering soil-structure interaction in the seismic design of building structures was introduced to capture soil-structure effects on the seismic performance of structures by proposing a response modification factor [15]. Also, an evaluation of the seismic performance of hypothetical tall buildings by estimating intensity measures, engineering demand parameters, and earthquake-induced losses using a soil-structure interaction numerical framework was carried out [16], and a new lateral load distribution pattern for seismic design of deteriorating shear buildings considering soil-structure interaction was introduced, demonstrating that the structures designed according to the proposed lateral force pattern experienced less damage than the code-conforming pattern [17].

Regarding the development of fragility curves, it should be noted that plotting and developing them for nuclear structures and facilities due to their high level of significance yet vulnerability at the time of earthquakes was the first application of these statistical tools in the field of structural engineering [18]. In 1993, these curves were developed further which at the time were considered primitive, simple, and mostly applicable based on experimental engineering judgment [19]. It can be asserted that it was after the devastating occurrence of Northridge earthquake in 1994 that greater attention was given to estimation of structural damage values and engineers started to focus greatly on predicting the amount of financial damages structures can bear at the time of facing extreme earthquake events. In 1994, over an extensive study of California's building structures, ATC-13 guidelines were used for development of fragility curves of more than 40 steel, reinforced concrete and wooden buildings of the state [20]. More recently, a study proposed empirical fragility curves of engineered steel and RC residential buildings after the devastating Mw 7.3 2017 earthquake in western part of Iran [21]. Seismic damage diagnosis in adjacent steel and RC MRFs considering pounding effects was investigated through improved wavelet-based damage-sensitive feature [22]. Seismic behavior assessment of steel moment-resisting frames under near-field earthquakes was carried out by evaluating seismic factors of response modifiers, ductility, overstrength, and deflection amplification [23]. In a novel study, development of fragility curves by using wavelet-based refined damage-sensitive feature considering higher mode contributions was carried out [24]. An investigation studied the integrated influence of both liquefaction and soil-structure interaction on the seismic response and vulnerability of low-code reinforced concrete moment-resisting frame buildings [25]. In another study, the influence of soil-structure interaction and nonlinear soil behavior on the seismic fragility of reinforced concrete dual (frame + shear wall) buildings resting on shallow foundations was investigated [26]. Analytical fragility curves of shallow-founded structures subjected to soil-structure interaction effects were developed, which indicated that consideration of soil-structure interaction increased the failure probabilities and highlighted the effects of the structural stiffness on the seismic vulnerability [27]. Simplified adjustment equations were proposed for estimating the collapse margin ratio of structures considering the soil-structure interaction effects [28]. A study investigating soil-structure interaction effects on seismic retrofit of soft first-story buildings through implementation of viscoelastic dampers indicated that the probability of structural failure significantly increased when soil-structure interactions were considered, and installation of viscoelastic dampers signifi-

cantly decreased the failure probability of the structure located on soft soil [29]. Also, seismic evaluation of special steel moment frames subjected to near-field earthquakes with forward directivity by considering soil-structure interaction effects was studied [30]. In another study, collapse probability of a seismically isolated reinforced concrete structure was investigated and findings showed that reducing the displacement capacity of isolators according to ASCE 7-16 caused the probability of collapse to exceed the 10% limit considerably, and the collapse probability of isolators was sensitive to ground motion suites [31]. The acceptability of monotonic and cyclic pushover analysis results for the near-collapse performance limit state was studied too, and cyclic pushover analysis was found acceptable for the near collapse performance limit state, whereas monotonic pushover analysis caused unacceptably high tensile and compression strains at the base columns, as well as large plastic rotations at the beams [32]. Clearly, there is still a considerable gap needed to be filled within this area owing to the rampant usage of moment-resisting steel frames, their seismic vulnerability, and the significant role of soil-structure interaction in capturing a better seismic performance of steel structures.

### 1.3. Aims and scopes

Amongst the moment-resisting steel frames, the intermediate type needs to be studied more, and by incorporating fragility curves, a better conclusion regarding its structural behavior at the time of earthquake can be achieved, especially if the effects of soil-structure interaction and height are also included, but evidently the number of such research studies about this particular type of structural system considering these two items is negligible within the current chapters of publications.

The purpose of this study is to investigate the effect of height on the seismic behavior of intermediate moment-resisting steel frame structures considering soil-structure interaction by employing the application of fragility curve, which is one of the most efficient methods in the structural performance assessment of building structures at different seismic levels.

In this research, three intermediate moment-resisting steel frame structures of 3, 6, and 9 stories are investigated. Incorporating method of plotting and developing the fragility curves of these structures is the IDA. In this method, 22 far-field ground motion records of FEMA-P695 were used and scaled to a specific acceleration. Ground motion records with different  $S_{aT1}$  (from zero to collapse of the structure) were applied, and scaling of the records was based on different  $S_{aT1}$  values. Each of these scaled records was applied to all three of these structures and their dynamic response was registered. Finally, by using probabilistic

methods, resulting responses were investigated and a set of fragility curves for each structure was developed.

## 2. Methodology

### 2.1. Investigated models

Moment-resisting steel frames are considered as commonly used structural systems that are preferably chosen for regions with medium to very high levels of seismic intensity. This system is designed based on three ductility levels of ordinary, intermediate, and special. Application of intermediate type is quite prevalent in the earthquake prone zones, but still a lower percentage of studies are carried out regarding this system compared to the special type; therefore, the type of moment-resisting steel frame used in this research is the one with an intermediate level of ductility.

In this study, 3 structures of 3-, 6-, and 9-stories are designed by CSI ETABS 2016 [33] according to the method of LRFD and based on ASCE7-16 consideration [34] using European steel profiles. Structures are considered to be designed in a region with a very high level of seismic intensity. Seismic design parameters of the assumed site are shown in Table 1. It should be mentioned that risk and seismic categories of the structures respectively are II and D. Structures are designed using time-history analysis and the employed design spectrum plotted by the seismic design parameters is presented in Figure 1. Investigated structures are regular both in plan and height with an area of 375 m<sup>2</sup> (15 m × 25 m) consisting of 3 spans of 5 m in X direction, 5 spans of 5 m in Y direction, and height of each floor considered equal to 3.2 m. Of note, in the process of calculating the required structural demands of each member, Demand-Capacity Ratio (DCR) of beams and columns was limited to 0.7–1.0 and 0.6–0.9, respectively, so that more than 85% DCRs of structural members stay within this interval. Plan and 3D view of each building structure are shown in Figure 2(a) to (d). Mechanical properties of the used steel are considered to be 2.0E5 MPa for modulus of elasticity, 240 MPa yield stress, 370 MPa ultimate

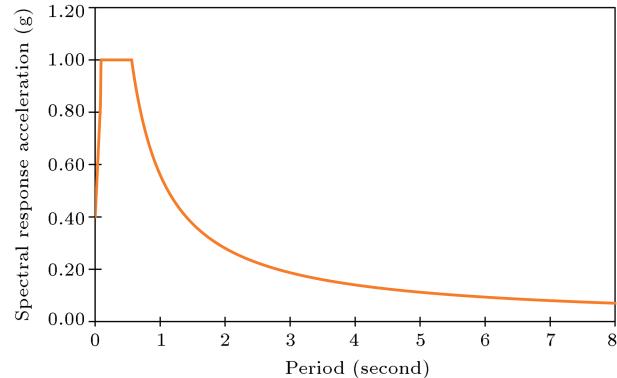


Figure 1. Design spectrum of the investigated models.

stress, and 0.25 ultimate strain. Regarding the mechanical properties of the used concrete, modulus of elasticity and compressive strength of it are equal to values of 2.0E4 MPa and 25 MPa. The type of soil considered in this research according to ASCE7-16 is type C, having a shear velocity of 360 m/s, internal friction angle of 42°, zero cohesion, elastic modulus of 2.0E11 MPa, shear modulus of 2.8E8 MPa, and dry density of 21 kN/m<sup>3</sup> [34]. Designed cross-sections and geometrical dimensions of the foundation of each structure are shown in Tables 2 to 5. Also, during the design procedure, at the bottom of columns in ground-zero elevation, the restraining condition is considered as rigid connections, and after extracting detailed forces of the structure, footings of the models were designed separately as strip foundations.

### 2.2. Incremental Dynamic Analysis (IDA)

In this study, IDA is used for the development of fragility curves. It is one of the special methods of

Table 2. Designed cross-sections of 3-story structure.

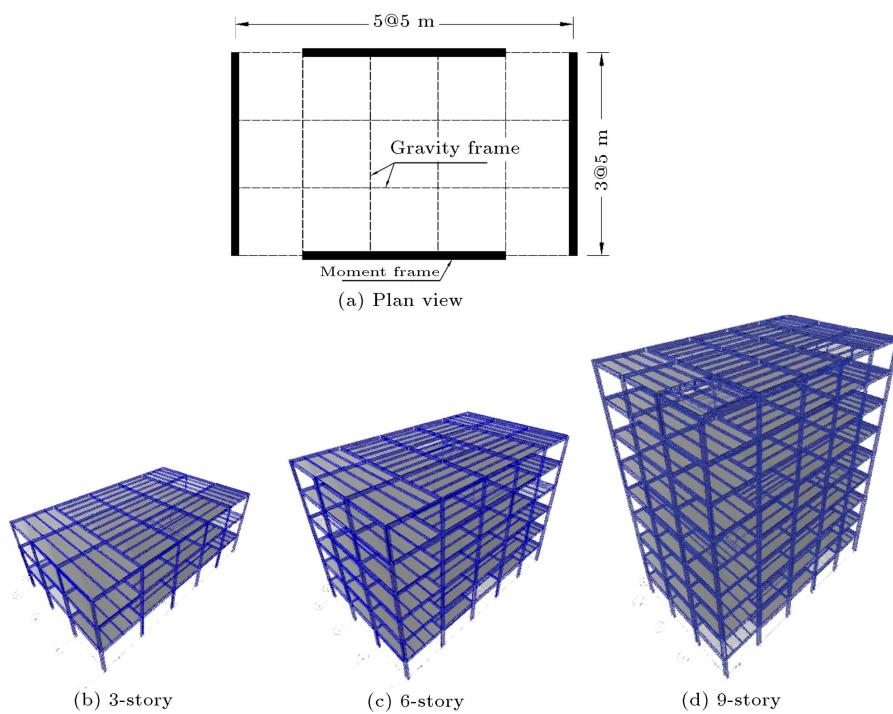
Structural elements	Stories		
	1st	2nd	3rd
MRF column	IPB320	IPB280	IPB220
Gravity column	IPB180	IPB160	IPB140
MRF beam	IPE400	IPE360	IPE330
Gravity beam	IPE330	IPE330	IPE330
Secondary beam	IPE220	IPE220	IPE220

Table 1. Seismic design parameters according to ASCE7-16 [34].

Parameters	Type or value
I (importance factor)	1
Site class	C
Risk category	II
Seismic design category	D
R	4.5
$S_s$	1.5
$S_1$	0.6

Table 3. Designed cross-sections of 6-story structure.

Structural elements	Stories		
	1st–2nd	3rd–4th	5th–6th
MRF column	IPB400	IPB320	IPB280
Gravity column	IPB240	IPB180	IPB160
MRF beam	IPE500	IPE450	IPE360
Gravity beam	IPE330	IPE330	IPE330
Secondary beam	IPE220	IPE220	IPE220



**Figure 2.** (a) Structural plan and (b)-(d) structural 3D views.

**Table 4.** Designed cross-sections of 9-story structure.

Structural elements	Stories		
	1st–3rd	4th–6th	7th–9th
MRF column	IPB550	IPB400	IPB320
Gravity column	IPB320	IPB240	IPB180
MRF beam	IPE550	IPE500	IPE400
Gravity beam	IPE330	IPE330	IPE330
Secondary beam	IPE220	IPE220	IPE220

**Table 5.** Geometrical dimension of foundations.

Structure	Strip foundation dimension ( width × length × height (m <sup>3</sup> ), depth (m))
3-story	1 × 16 × 0.7 m <sup>3</sup> , 1.2 m
6-story	1.5 × 16.5 × 1.0 m <sup>3</sup> , 1.5 m
9-story	2 × 17 × 1.3 m <sup>3</sup> , 1.8 m

nonlinear dynamic analysis that uses a set of nonlinear time history analyses, applies records to the structures until the collapse point, and simplifies the comparison of the structure's seismic capacity with its demand. In this procedure, a set of records with different scaled levels of intensity is applied to a structure, and after nonlinear analysis, a number of intensity level-response graphs would be produced that include all the structural behavior spectra, and by introducing limit states plus adding results to analytical probabilistic graphs, structural assessment can be carried out. With

the application of this method, targeted structure undergoes a gradual change of behavior from linear elastic to dynamic instability, which results in an accurate and reliable estimation of collapse capacity of the structure. Many researchers have contributed to the development of this method [35,36], and it has been used as an innovative procedure in determining structural collapse capacity by FEMA manual since 2000 [37].

The first stage of this procedure is understanding the inputs and outputs, according to Pacific Earthquake Engineering Research Centre's guidelines [38]. A parameter named Intensity Measure (IM) must be chosen by seismic risk analysis of the desired region in order to be applied to the structure, and at the subsequent stage, a corresponding structural response to each IM or Damage Measure (DM) is achieved which would be considered as an Engineering Demand Parameter (EDM). Finally, based on a pre-defined damage indicator, collapse probability can be calculated which can be used for cost estimation of structural rehabilitation. Thus, IDA curves are a set of IM-EDP graphs whose probabilistic studies can be accomplished by them.

IM is a scalable quantity of a record. In this study, records' spectral acceleration corresponding to the first mode of the structure with damping ratio of 5% ( $S_a(T_{1,5\%})$ ) was chosen to be more efficient to be used as the correct input for extracting the IDA curves because they have far less data scattering compared with other quantities like Peak Ground Acceleration

(PGA). Regarding the DM as the output of the IDA procedure, maximum inter-story drift ratio is the chosen DM used for the analysis of IDA curves.

### 2.3. FEMA-P695 ground motion records

One of the accredited sources for recommendation of ground motion records for seismic assessment is the FEMA-P695 manual [1]. This guideline divides the records into two categories of far-field earthquakes recorded with the distance of more than 10 km from the fault and near-field earthquakes recorded from the distance of less than 10 km from the fault. According to this manual, the criterion of distance between the locations of recording the earthquake and the fault is the average distance of Junior-Bohre and Campbell. In this research, a set of 22 far-field ground motion records of FEMA-P695 with magnitudes between 6.5 and 7.5 Richter distanced more than 10 km from the fault is used. Table 6 indicates the employed records in this study with their name, magnitude, and year of occurrence.

**Table 6.** Far-field ground motion records of FEMA-P695 [1].

Ground motion records				
No.	RSN*	Name	Year	M (Richter)
1	953	Northridge, USA	1994	6.7
2	960	Northridge, USA	1994	6.7
3	1602	Duzce, Turkey	1999	7.1
4	1787	Hector Mine, USA	1999	7.1
5	169	Imperial Valley, USA	1979	6.5
6	174	Imperial Valley, USA	1979	6.5
7	1111	Kobe, Japan	1995	6.9
8	1116	Kobe, Japan	1995	6.9
9	1158	Kocaeli, Turkey	1999	7.5
10	1148	Kocaeli, Turkey	1999	7.5
11	900	Landers, USA	1992	7.3
12	848	Landers, USA	1992	7.3
13	752	Loma Prieta, USA	1989	6.9
14	767	Loma Prieta, USA	1989	6.9
15	1633	Manjil, Iran	1990	7.4
16	721	Superstition Hills, USA	1987	6.5
17	725	Superstition Hills, USA	1987	6.5
18	829	Cape Mendocino, USA	1992	7.0
19	1244	Chi-Chi, Taiwan	1999	7.6
20	1485	Chi-Chi, Taiwan	1999	7.6
21	68	San Fernando, USA	1971	6.6
22	125	Friuli, Italy	1973	6.5

\*RSN: Record Serial Number

### 2.4. Soil-Structure Interaction (SSI)

Normally, when building structures are going to be designed, the SSI is not considered in their design process, and to be more clear, the nonlinear response of shallow foundations in the event of seismic excitation due to complexity of the issue and computational hardship is quite cost-effective during the design process of ordinary building structures, but in the research fields, many scholars have contributed to the subject of SSI resulting in various experimental and numerical studies concerned with investigating the inelastic response of shallow foundations caused by earthquake [39–41]. Amongst the most common methods of SSI analysis such as continuum mechanics methods (FEM, BEM), macro elements and Winkler method, or “the Beam on Nonlinear Winkler Foundation (BNWF)” method, the BNWF is chosen for this study since it requires much less computational resources and time than other methods [42]. This method uses a set of distributed, vertical, and inelastic springs along the length of the footing; is capable of changing the stiffness of the springs, modeling the footing pullups, applying nonlinear soil properties, and modeling rocking displacement; and is able to consider radiation damping [43,44]. In the performance-based design approach, the designed structure must accomplish its targeted objectives, and soil-structure interaction as one of most important targets in structural performance due to its uncertainties must be dealt with considerably. Performance-based codes and manuals such as FEMA-P695 and ATC-40 recommend the consideration of SSI in the design process using simplified yet reliable method of BNWF based on taking into account the effect of pullup, soil, and foundation stiffness with considering uncertainties for different types of soils [42,45].

### 2.5. OpenSees simulation

OpenSees as a finite element method software package, which is still under development, presents a fast, reliable, and simple mean of simulation through its code scripts; it is comprised of three parts: Model building, analyzing, and recorder [46].

In the simulation process through OpenSees, structural models' geometry, boundary conditions, and material properties of steel were defined according to the designed models by CSI ETABS. The “Fibre” section was selected for the model and “NonLinear Beam-Column” as the appropriate structural element. Due to the simplicity of modeling beam-column steel panel zones, panel zone “Scissor” models with nonlinear spring elements were used [47]. For the simulation of SSI, as it was stated, the BNWF was considered as a proper method. Required parameters of BNWF method are comprised of type of soil (sand or clay), foundation's capacity (vertical and horizontal), foundation's dimensions (width, length and height), foun-

dation's stiffness (vertical and horizontal), placement of vertical springs (distance and position), radiation damping, and tensile capacity. The considered type of soil in this study is type C, which mostly consists of sand and gravel, typically to be the least stable soil. For calculating the vertical and horizontal bearing capacities of the designed foundation, Meyerhof equations as stated below were used [42]:

$$Q_{ult} = CN_c F_{cs} F_{cd} F_{ci} + \Upsilon D_c N_q F_{qs} F_{qd} F_{qi} \\ + 0.5 \Upsilon B N_\Upsilon F_{\Upsilon s} F_{\Upsilon d} F_{\Upsilon i}, \quad (1)$$

$$T_{ult} = W_g \tan \delta + A_b C, \quad (2)$$

where  $Q_{ult}$  and  $T_{ult}$  are the vertical and horizontal bearing capacities, respectively;  $N_c$ ,  $N_q$ , and  $N_\Upsilon$  are bearing coefficients;  $F_{cs}$ ,  $F_{qs}$ , and  $F_{\Upsilon s}$  are shape coefficients;  $F_{cd}$ ,  $F_{qd}$ , and  $F_{\Upsilon d}$  are depth coefficients;  $F_{ci}$ ,  $F_{qi}$ , and  $F_{\Upsilon i}$  are loading slope coefficients;  $W_g$  is total weight;  $\delta$  is the friction angle between footing and soil equal to  $1.3\varphi - 2.3\varphi$ ; and  $A_b$  is footing's bottom area.

Foundation dimensions as designed are mentioned in Table 4, and stiffnesses of the foundations are calculated according to Gazetas equations as in the following as recommended by FEMA-P695 [1] and ATC-41 too [42]. However, since the proposed structural models are simulated 2-dimensionally, only vertical stiffness along  $Z$ -axis, rotational stiffness along  $Y$ -axis, and horizontal stiffness along  $X$ -axis are required. It must be noted that the sum of springs' vertical stiffnesses under the footing must be equal to total elastic stiffness, and also the total rotational stiffness must be equal to the sum of rotational stiffnesses produced via vertical springs along the footing where in case of our simulation, both of these conditions were checked out correctly [42].

$$K_i = K'_i e_i, \quad (3)$$

where  $K_i$  is total elastic stiffness;  $K'_i$  is uncoupled total surface stiffness consisting of  $K'_z$ ,  $K'_{\theta y}$ , and  $K'_{\theta x}$ ; and  $e_i$  is stiffness embedment factor consisting of  $e_z$ ,  $e_{\theta y}$ , and  $e_x$ .

Also, since BNWF method is not sensitive to the issue of horizontal distance of the springs (not mesh sensitive) [48], a distance of 25 cm was considered to be implemented for the placement of springs along the footings. Regarding the radiation damping, it was suggested that it only overestimated the structural behavior to a negligible value; thus, a damping ratio of 5% is considered for the soil in the simulation process [49], and considering the properties of the type of soil studied in this research, tensile capacity is considered zero.

For the purpose of assigning the discussed soil properties to the predefined springs by BNWF method in OpenSees, two nonlinear material models of Qzsimplle and Tzsimplle introduced by Boulanger [43] were

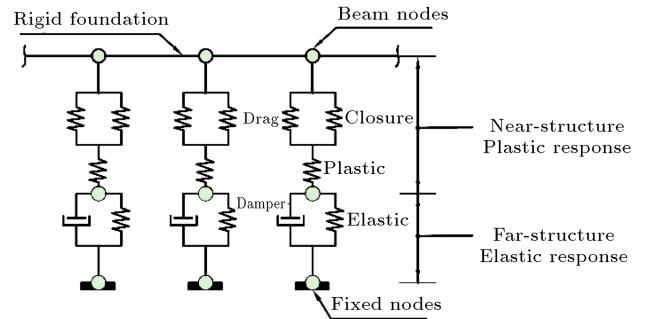


**Figure 3.** Method of employing the Winkler springs using ZeroLength elements [42].

employed which were capable of modeling the load-displacement and shear-sliding behavioral curves, respectively. The appropriate element for simulating the vertical and horizontal springs is an element with zero length, titled ZeroLength element, which by using it, two points with the same coordination but different degrees of freedom can be connected, and the most important aspect of this element is its zero length [42]. Thus, by using this element, material models of Qzsimplle and Tzsimplle were assigned to the vertical and horizontal degrees of freedom of this element and these elements were implemented as the vertical and horizontal Winkler springs along the footing. Figure 3 illustrates how to employ Qzsimplle and Tzsimplle sequentially along a simulating footing [42]. As shown, each node located on the rigid foundation is coinciding by ZeroLength elements with its corresponding node on the beam, which is considered the footing itself, and both of these two nodes have the same coordination. All the nodes at the base level are restrained in all degrees of freedom, and material model of Qzsimplle is assigned to their corresponding ZeroLength elements. In addition, the beam at its both end length as footing is restrained horizontally using a ZeroLength element equipped with Tzsimplle material model which besides stabilizing the simulated structure presents modeling the horizontal behavior (sliding) of the footing substructure.

## 2.6. 2D simulation

Based on the procedure and details discussed, simulation of the proposed models was carried out by means of OpenSees software [46]. According to a recommendation, considered seismic mass of structures was set equal to  $1.05DL + 0.5LL$  [50]. As it was stated before, designed structural models are simulated two-dimensionally in OpenSees in which a circumferential moment-resisting frame from each model is selected for simulation, and the effect of the third dimension of the structure (especially in the presence of lateral loads) is neglected; hence, for taking it into consideration in the simulation process, a technique commonly known as addition of the “ $P-\Delta$  column” or “leaning column” to 2D models is used. It is also essential to apply the

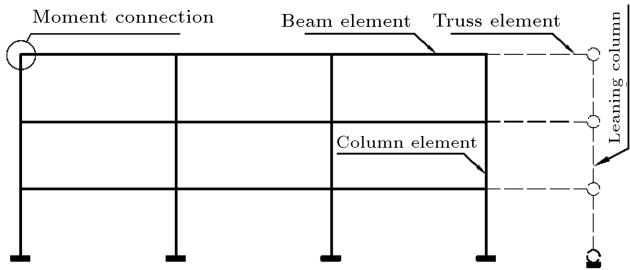


**Figure 4.** Implementation of leaning column in a 3-story structure.

true mass of each frame because it leads to achievement of correct results. Thus, for each floor of the 2D models, the mass of frames is calculated at story levels and assigned to elemental nodes. As is shown in Figure 4, gravity columns are located on a row with hinge joints on the right side of frame being connected to the structure using “truss” elements. Section area and moment of inertia of gravity columns are equal to the eliminated columns from the 3D model frame. Moreover, in the numerical simulation done using OpenSees software [46], cyclic degradation is considered which is part of the material assignment procedure. The “uniaxialMaterialSteel02” attribute in OpenSees features the cyclic material degradation embedded within itself, which was assigned as steel material to the structural element.

## 2.7. Verification

For the purpose of validating the simulated models, considering both linear and nonlinear structural behaviors, two consecutive approaches are followed; firstly, for linear verification, structural period of the design models are compared with the simulated ones; then, for the purpose of verifying structural models considering the nonlinear structural behavior, simulated models are compared with experimental results.

Structural modes (1st mode) of the simulated models using OpenSees and designed models by CSI ETABS are compared with each other, showing that values are in acceptable agreement. Table 7 shows the fundamental periods of simulated and designed models of the three structures with rigid foundations along with the fundamental periods of simulated models with and without consideration of SSI which clearly

**Table 7.** Comparison of the fundamental period of designed and simulated models with and without Soil-Structure Interaction (SSI) consideration.

Models	$T$ (sec) (ETABS)	$T$ (sec)	
		(OpenSees) With SSI	(OpenSees) Without SSI
3-story	0.989	1.06	0.993
6-story	1.447	1.51	1.454
9-story	1.752	1.803	1.776

indicates that SSI consideration increases (though negligible) the fundamental period of the models in comparison with models having rigid foundation. This comparison justifiably verifies the linear performance of the models, but still lacks proper nonlinear validation.

Suita et al. [51] studied a 4-story steel structure experimentally subjected to earthquake records on a shake table facility at Japan’s Defense Center and investigated its behavior until the stage of total collapse. The tested structure was designed according to seismic standard codes of Japan; a complete description of the material properties and sections used in this structure is fully given in the referenced research paper [51]. Figure 5(a) shows the overall view of the tested model.

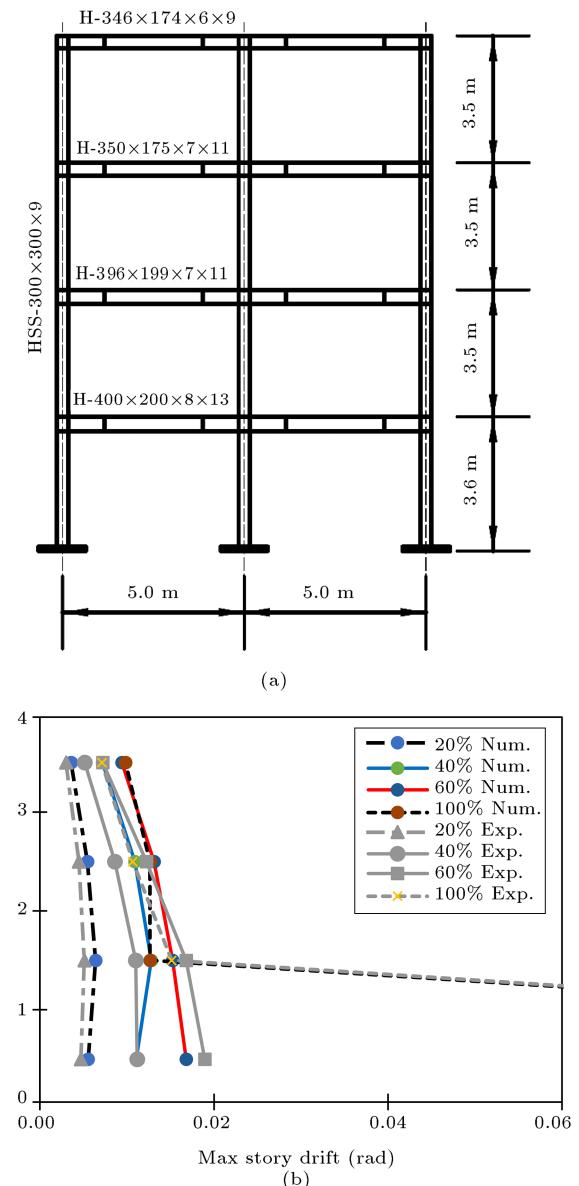


**Figure 5.** (a) Steel structure model on shake table tested at Japan Defense Center [51]. (b) Comparison of 2D model’s results with experimental test.

Kobe earthquake record registered at Takatori station was used as seismic load on this structure, and it was reported that the structure collapsed due to continuous failure (side-sway) on the 1st story. In addition, Lingos et al. [52] conducted a study to produce a validated analytical model for collapse assessment for steel structures based on the results of this experiment. By representing accurate results, Lingos et al. [52] stated that the verified models could surely assess structural collapse. Also, they came to a conclusion that no significant advantage was observed in using 3D or 2D model regarding the assessment of a structure's collapse potential. In this research, two spans of this 4-story structure was modeled 2-dimensionally and as stated previously, plastic torsional springs were employed in the elements and the effect of slab over beams and columns was simply neglected. This 2D model was simulated by OpenSees and subjected to Kobe earthquake record in the Eastern-Western (EW) direction at 4 acceleration levels of 20%, 40%, 60%, and 100% as described in the experimental test, and maximum story drifts of the structure were compared with experimental data. Results of Lingos et al. [52] were in perfect agreement with the experimental ones, so are the results of this research. Figure 5(b) indicates the results of simulated models with experimental data. So, based on this verification used for the proposed structural models in this study, 2D structural models simulated using OpenSees are concluded to be validated.

### **2.8. Performance levels**

Performance levels and limit states are two important factors essential to be taken into account in the seismic performance-based design of structures, which can be extracted from IDA curves. Of course, the data derived from these graphs must be narrated mathematically; for instance, DM can be used as a damage criterion capable of being described through test, theory, and even engineering judgment.

One of the crucial points in performance levels, which is significant in structural assessment, is the collapse point of a structure and it is considered to be vital in predicting structural collapse. ASCE/SEI 41 states that collapse occurs when one structural element carries loads more than its collapse point capacity [53]. In most cases, exceeding this collapse point demand does not trigger any structural instability or collapse, but it is a conservative term used for structures close to the brink of collapse. Moreover, FEMA-350 guideline describes the collapse point or collapse prevention point for steel structures based on IDA curve, accordingly defining collapse point as a point in the curve in which its slope tangent is 20% of the initial elastic slope, or a point of the curve in which inter-story drift reaches 10% of  $H$  in which  $H$  is the story height. This method

considers the horizontal adaptation of IDA curves as a sign of structural dynamic instability [3].

In this study, collapse is defined as a point in which structure experiences instability and undergoes the state of collapse or beyond it; thus, based on this definition, two sets of structural collapse condition are chosen for our analysis. The first one defines the collapse prevention point by the intensity of the ground motion in which inter-story drift increases exceedingly with a small growth of ground motion's intensity. This phenomenon is observed in IDA curves by its leveling off.

The second means of determining structural collapse is by employing DM criteria in IDA curve also called collapse by non-simulated modes. Generally, maximum inter-story drift is considered for assessment of structural collapse, and exceeding the limited value of it plus accompanying it with gravitational loads and  $P - \Delta$  effect will trigger the collapse of a structure. For defining limit states and measuring the value of the inter-story drift at the point of collapsing, nonlinear static analysis (pushover) is required for simulating the collapse and achieving maximum inter-story drift for unstable states of the structure [5]. It is concluded from the studies on the nonlinear static analysis of moment-resisting frames that roof's average drift equals 8–10% of the frame's shear capacity and the roof's drift approximately equals 15% of inter-story drift. Thus, by defining a limit state of 1–8–20% as the inter-story drift, the collapse prevention point will be set far more than the unstable state of structure [54]. In this case, structural collapse must be determined explicitly by defining a limit state rather than a simple point, in which case numerical simulation results in divergence. Due to the ambiguity in previous researches regarding inter-story drift and divergence of responses in higher inter-story drifts, studies have generated very conservative estimations of limit states and structural collapse capacity, but the convergence of responses depends greatly on the solution's algorithm.

Since dynamic instability is eliminated by solution algorithm resulting in convergence of structure in top drifts, in this study, collapse prevention point for each record is defined by the corresponding  $S_a$  (spectral acceleration) with the horizontal line of IDA curve or simply when the inter-story drift reaches 10%.

### **2.9. Development of fragility curves**

There are different methods of assessing the seismic vulnerability of structures varying based on their required computational time and accuracy; however, amongst such methods, using fragility curves method is more common in practice since it considers the exceedance probability as a function of ground motion's characteristic and design parameters. For the purpose of extracting fragility curves, a probability distribution

for achieved Engineering Demand Parameters (EDPs) at each corresponding IM in nonlinear dynamic analyses must be employed. Mean and standard deviation for each one of the EDPs are calculated for considering the effect of earthquake records' summation; then, by using cumulative distribution function, exceeding the probability of each one of EDPs from the considered limit states will be calculated [55].  $P(C/IM = X)$  represents the exceedance probability from a performance level at a specified IM [55]:

$$P(C/IM = X) = \Phi\left(\frac{\ln(x/\theta)}{\beta}\right), \quad (4)$$

$$\ln(\theta) = \frac{1}{n} \sum_{i=1}^n \ln(IM_i), \quad (5)$$

$$\beta = \sqrt{\frac{1}{n-1}} \sum_{i=1}^n \left( \ln \left( \frac{IM_i}{\theta} \right) \right)^2, \quad (6)$$

where  $\theta$  is the mean of the fragility function (IM level with 50% probability) and  $\beta$  is the standard deviation of  $\ln(IM)$ .

Eq. (4) states IM values that trigger exceedance from a performance level at a specified IM and do have normal distribution.

In this study, values of seismic intensity for both cases of fixed and flexible bases for 3-, 6-, and 9-story structures are approximately considered 0–3.5 g, 0–3 g, and 0–2.5 g, and probabilities of exceeding the performance levels of IO, LS, and CP are set to change between 0 and 1, and maximum drift values reaching each of these three levels are considered 0.7%H(0.007H), 2.5%H (0.025H), and 5% (0.05H), respectively, in which  $H$  is the story height [3]. For each structure under far-field records, the possibility of comparing their probabilistic assessment against each performance level is discussed through fragility curves. By using achieved IDA curves ( $S_{a(T1,5\%)}$  – maximum drift ( $H$ )) and employing normal probability distribution at each maximum drift based on specified IM, desired fragility curves are plotted.

### 3. Discussion of the results

#### 3.1. IDA curves

IDA procedure for 3 structural models of 3, 6, and 9 stories with rigid and flexible foundations produces ( $S_{a(T1,5\%)}$ –maximum drift ( $H$ )) curves, as shown in Figure 6.

It can be understood from the IDA curves of structures with rigid and flexible foundations that the coefficient of  $S_{a(T1,5\%)}$  tends to increase its nonlinearity with more intensity and the decline of height, and the increased height of structures generates nonlinear

responses with less intensity than lower-rise structures. Since lower-rise structures have a shorter time period, the corresponding design forces of such structures tend to be greater than forces that higher-rise structures must transfer.

#### 3.2. Application of performance levels on IDA curves

The concept of performance level is of paramount importance for the development of fragility curves. In FEMA-350 guideline, 3 performance levels titled as Immediate Occupancy (IO), Life Safety (LS), and Collapse Prevention (CP) are introduced, which correspond to inter-story relative displacements (drift) of 0.7%H (0.007H), 2.5%H (0.025H), and 5% (0.05H), respectively, in which  $H$  is the story height [3]. Figure 7 illustrates the method of determining the performance levels on IDA curves. Performance level of IO corresponds to a level of damage that structure is safe for occupancy after earthquake, while the performance level of LS defines a state in which structure indeed experiences damage considerably, but the risk of life-threatening dangers for occupants still remains low. Finally, the level of CP describes a condition where structure is on the brink of total or minor collapse due to lateral loads, but still can maintain its capability to resist collapse [4].

#### 3.3. Uniformed IDA curves

At this stage, extracted IDA curves must be uniformed using median values. Curves of IDA16%, IDA50%, and IDA84% are generated for each structure with and without SSI consideration. IDA16% curve is the uniformed median minus 34% deviation, IDA50% curve is the uniformed median, and IDA84% curve is the uniformed median plus 34% deviation.

For performance comparison of these 3 types of structures possessing different design settings, damage intensity, and structural performance, in the IDA curves,  $S_{a(T1,5\%)}$  must be scaled to  $S_{a(\text{Design})}$  (design spectral acceleration). Figure 6 shows a summary of IDA50% curves scaled to  $S_{a(\text{Design})}$ . It is well understood from the graph that 3-story structures have less strength against selected records scaled to  $S_{a(\text{Design})}$  than 6-story and 9-story structures, and by comparing the median of structures with rigid foundation (fixed base) and structures with SSI consideration, it is clear that SSI consideration tends to tolerate lower spectral accelerations. When the median value of  $S_{a(T1,5\%)}/S_{a(\text{Design})}$  is equal to one, 6-story and 9-story structures have less relative displacement than 3-story structures but greater values of spectral acceleration, as stated in Table 8. For instance, 3-story structures with and without SSI consideration reach the LS performance level at  $S_{a(T1,5\%)}/S_{a(\text{Design})}$  equal to 1.05 and 1.13, respectively, which are less than

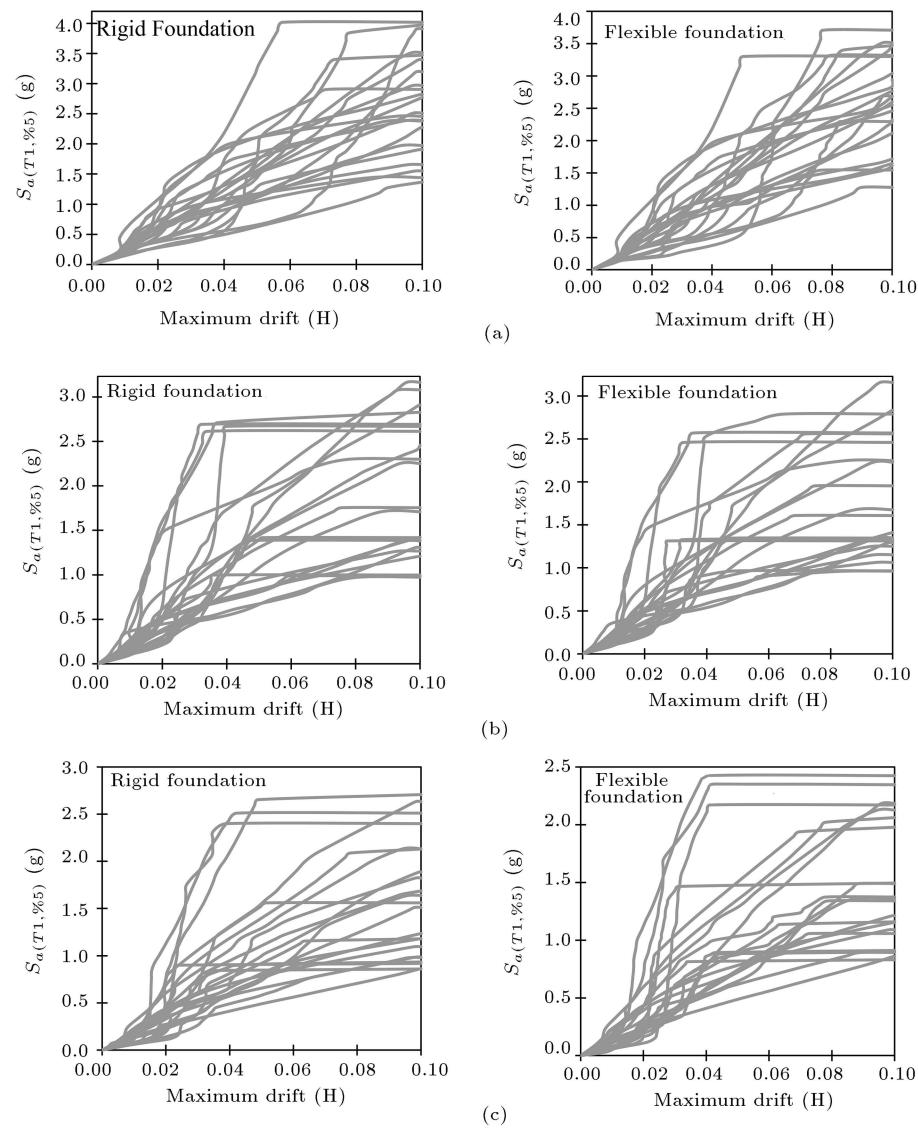


**Figure 6.** IDA curves for structures with rigid and flexible foundations of (a) 3-story, (b) 6-story, and (c) 9-story.

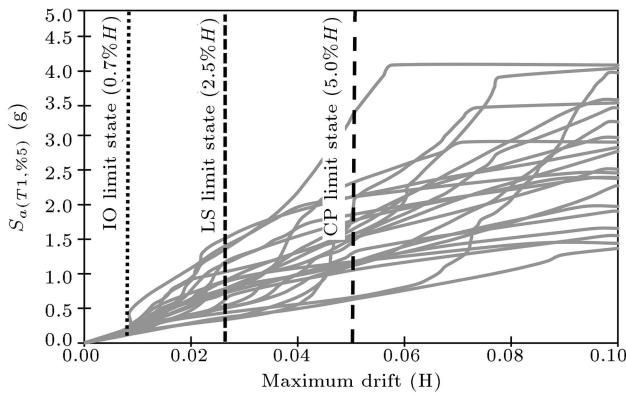


**Figure 7.** Performance levels on IDA curves.

the corresponding ones for 6- and 9-story structures. It needs to be noted that for both conditions with and without SSI consideration,  $S_{a(T1,5\%)}$  is scaled to  $S_{a(\text{Design})}$ . In fact, for structures with SSI consider-

ation,  $S_{a(T1,5\%)}$  must be scaled to  $S_{a(\text{Design})}$  that is consistent with the structure's time period. Moreover, Figure 8 illustrates that curves of structures with SSI consideration are plotted lower than structures with fixed base; this clearly shows the undesirable effect of SSI consideration at a specific spectral acceleration; however, since the application of SSI consideration corresponds to lower spectral accelerations, it can be useful in reduction of drifts and produced structural forces.

#### 3.4. Comparison and modification of fragility curves

Based on the results, fragility curves of structures with SSI consideration for all the 3 types are plotted higher than fixed base structures; thus, by having these fragility curves, exceedance probability for designed structures with both conditions can be calculated

**Table 8.** Median values of  $S_{a(T1,5\%)} / S_{a(\text{Design})}$  for structures with and without SSI consideration at different performance levels.

Fixed base	IO	LS	CP	SSI consideration	IO	LS	CP
3-story	0.21	1.13	2.28	3-story	0.21	1.05	2.14
6-story	0.31	1.86	3.45	6-story	0.29	1.67	3.22
9-story	0.26	1.71	3.30	9-story	0.23	1.61	3.30

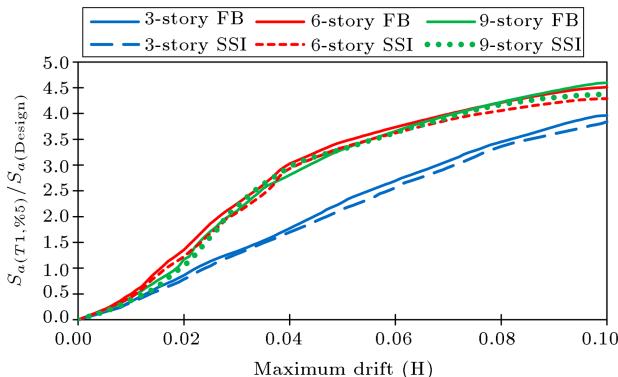


**Figure 8.** Summary of IDA50% curves scaled to  $S_{a(\text{Design})}$  for all 3 types of structures having fixed base with SSI consideration.

according to standard code consideration, fundamental time period, and specific soil type. Comparison of the results of these two conditions proves that exceedance probability for frame structures with SSI consideration increases for one specified spectral acceleration. This issue remarks the negative effect of SSI consideration on collapse behavior of studied frame structures. Consideration of SSI increases the structure's fundamental period, which causes spectral acceleration to decline. Also, it must be mentioned that collapse spectral acceleration for each frame is determined based on the structure's time period for both conditions of fixed and flexible bases, and these spectral accelerations are absolutely not the same. Thus, basically, the comparison is wrong due to lack of the same  $S_{a(T1,5\%)}$ . Results from developed fragility curves for structures with fixed and flexible bases show that the latter meet the same collapse criterion at lower spectral accelerations. For understanding exceedance probability of the structure with flexible base, it must be read at lower probabilities. Unmodified fragility curves show that the spectral acceleration corresponding to the curve with SSI consideration has higher exceedance probability than the case with the fixed base. This can be ambiguous and complex to read; thus, to make a correct comparison, collapse spectral accelerations must be modified first; then, a comparison should be carried out at equal spectral accelerations.

For the purpose of modifying collapse spectral accelerations in both of the specified cases, a graph, shown in Figure 9, is plotted which indicates corresponding points to collapse spectral accelerations of

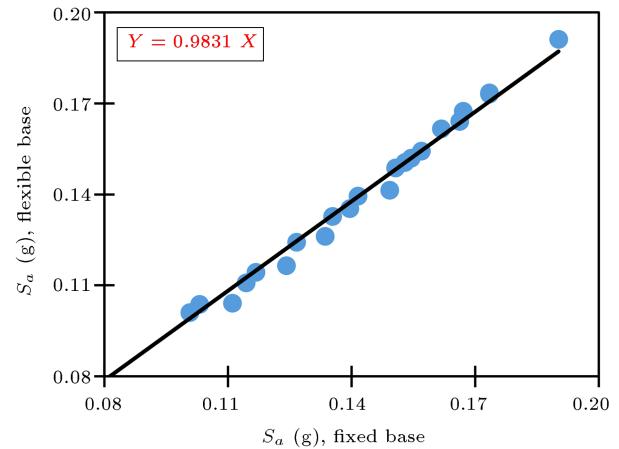


**Figure 9.** Modification coefficient of spectral acceleration for a 3-story structure with flexible base at the performance level of IO.

structures with fixed and flexible base at the performance level of IO. This graph shows the relationship between these two accelerations.  $X$  axis of this graph denotes collapse spectral acceleration of cases with fixed base and  $Y$  axis shows collapse spectral accelerations of cases with flexible base. Driven slope of this curve represents the correlation of these two cases. Since frame structures with fixed base reach the collapse criterion with higher spectral accelerations compared with flexible base ones, slope of this curve is always less than one. So, for modifying collapse spectral acceleration of flexible base cases, all the accelerations must be multiplied by the inverse ratio of the curve's driven slope at different performance levels which are shown in Table 9.

Based on the results achieved from modified fragility curves shown in Figure 10, it is observed that modified fragility curves of cases with SSI consideration (flexible base) are rightly resisting against higher spectral acceleration and are located lower than fragility curves of fixed base cases, thus leading to lower exceedance probability. Horizontal axis presents

**Table 9.** Modified median values of  $S_{a(T1,5\%)} / S_{a(\text{Design})}$ .

Modified SSI consideration	IO	LS	CP
3-story	0.9831	0.9327	0.962
6-story	0.9005	0.8796	0.9232
9-story	0.9188	0.8725	0.8356

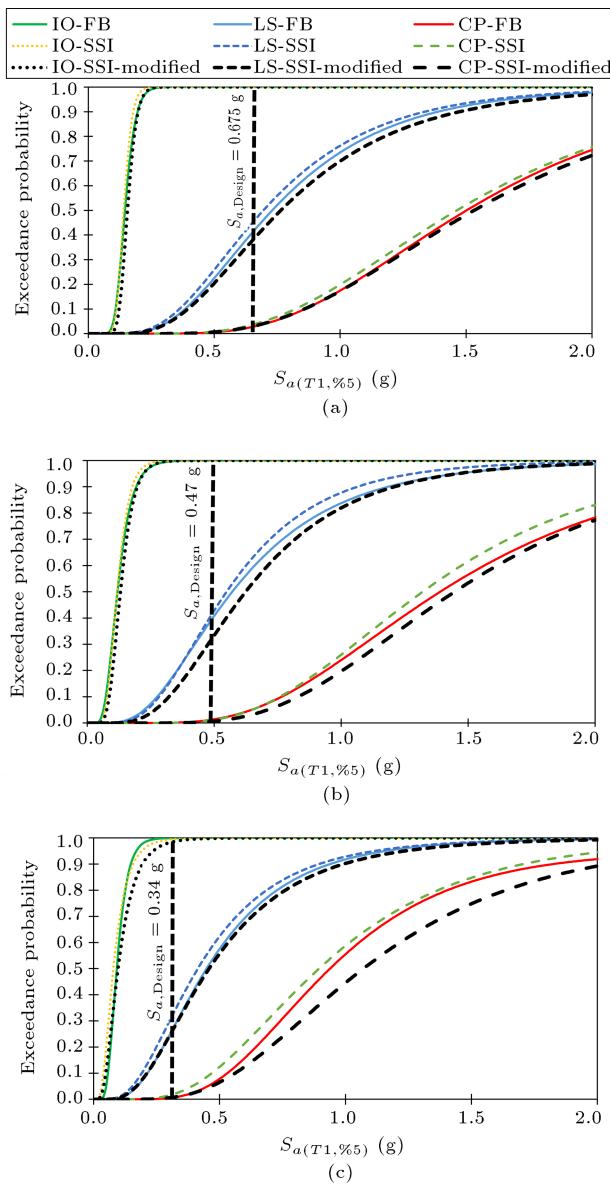


**Figure 10.** Modified fragility curves of (a) 3-story, (b) 6-story, and (c) 9-story structures.

IM or  $S_{a(T1,5\%)}$  and vertical axis denotes exceedance probability based on performance levels of CP, LS, and IO. Fragility curves of each structure with and without SSI consideration are compared separately. Red, blue, and green curves represent the probability of exceeding performance levels of CP, LS, and IO for structures

with fixed base, respectively, and dotted orange, blue, and black curves indicate the probability of exceeding the performance levels of CP, LS, and IO for structures with SSI consideration. Plotted fragility curves at different performance levels show that lower-rising structures tend to collapse with higher  $S_{a(T1,5\%)}$  while the proposed high-rise structures adapt to structural collapse with lower spectral accelerations of the first mode. Comparison of these two sets of curves indicates that exceedance probability is decreased for structures on flexible bases, thus illustrating the positive effect of SSI consideration on collapse behavior of the studied frame structures. Using these curves with the principal time period in the fixed base case, exceedance probability in the case of flexible case can be achieved by spectral acceleration from the modified fragility curves.

### 3.5. Exceedance probability using spectral design acceleration, $S_{a(\text{Design})}$

Figure 10 shows the modified fragility curves of each structure derived from specified performance levels that are specially noted by the calculated spectral design acceleration of each structure. In addition, Table 10 indicates exceedance probability of each structure at the defined performance levels based on specific spectral design acceleration.

As can be understood from this figure and table, structures with SSI consideration reach the performance levels later than the fixed base structures with lower exceedance probabilities. In other words, the SSI consideration leads to the reduction of exceedance probability. For instance, 3-, 6-, and 9-story structures at the time of earthquake occurrence with spectral acceleration equal to  $S_{a(\text{Design})}$  reach the performance level of LS with probability values of 0.45, 0.38, and 0.32 for cases with fixed base and 0.41, 0.30, and 0.23 for cases with SSI consideration, respectively. Also, Figure 10 clearly indicates that in the case of performance levels of LS and CP at respective spectral accelerations intervals of 0.25 to 2 and 0.5 to 2, SSI consideration leads to lower exceedance probability values for all the investigated models than fixed base ones. In addition, with the increase in height, the exceedance probability for both of the fixed and flexible cases is reduced, thus pointing to the indirect correlation between height and exceedance probability.

**Table 10.** Exceedance probability for structures with fixed and flexible bases at  $S_{a(T1,5\%)} = S_{a(\text{Design})}$  specified for each model.

Exceedance probability (fixed base)	IO	LS	CP	Exceedance probability (flexible base)	IO	LS	CP
3-story	1	0.45	0.03	3-story	1	0.41	0.025
6-story	1	0.38	0.02	6-story	1	0.30	0.015
9-story	1	0.32	0.01	9-story	1	0.23	0.008

#### 4. Summary and conclusions

This study investigated the effect of soil-structure interaction and height on the development of fragility curves for moment-resisting steel frame structures. Structures were considered as intermediate moment-resisting steel frames with different heights from low to mid rise (3, 6, and 9 stories). Twenty-two far-field ground motion records of FEMA-P695 guideline were applied to models and subsequently were analyzed by IDA method. Results of this study consisted of IDA and fragility curves, indicating the probability of reaching three performance levels of IO, LS, and CP based on different IMs and then, results for each structure were compared. The following statements are the summaries of the perceived results:

1. Investigating the seismic performance of structures using fragility curves was considered as one of the efficient methods for assessment of structural vulnerability;
2. According to the presented results from fragility curves regarding damage level at various performance levels, these curves can be used as an effective engineering judgment tool for structural collapse assessment;
3. Designed structures according to referenced seismic standard codes against far-field records could be prone to higher vulnerability as height decreased;
4. IDA50% curves showed that the corresponding  $S_{a(T1,5\%)} / S_{a(\text{Design})}$  to reach performance levels of IO (Immediate Occupancy), LS (Life Safety), and CP (Collapse Prevention) for 3-, 6-, and 9-story structures with SSI consideration were 0.21, 0.32, 0.26; 1.13, 1.89, 1.80; and 2.29, 3.49, 3.96, respectively, while the same values for structures without SSI consideration were 0.19, 0.30, 0.25; 1.12, 1.86, 1.71; and 2.28, 3.45, 3.30. It was found that values of  $S_{a(T1,5\%)} / S_{a(\text{Design})}$  for 6- and 9-story structures were more than those for 3-story structures and SSI consideration increased  $S_{a(T1,5\%)} / S_{a(\text{Design})}$  values compared with the fixed base cases;
5. Higher-rise structures in this research had record induced  $S_{a(T1,5\%)}$  closer to  $S_{a(\text{Design})}$  and with decrease in height, the difference tends to increase;
6. Overall, SSI consideration produces the following desirable results:
  - Exceedance probabilities for 3-, 6-, and 9-story fixed base structures of at the performance level of LS at the acceleration equal to each structure's specific  $S_{a(\text{Design})}$  were 0.45, 0.38, and 0.32, while the same values for structures with SSI consideration were 0.41, 0.30, and 0.23. This clearly indicates that exceedance probability decreases with increase in the structure's height and SSI

consideration adapts to lower exceedance probability for the studied structures;

- Exceedance probabilities for 3-, 6-, and 9-story fixed base structures of at the performance level of CP and at an acceleration equal to each structure's specific  $S_{a(\text{Design})}$  were 0.03, 0.02, and 0.01, while the same values for structures with SSI consideration were 0.025, 0.015, and 0.008. This clearly indicates that exceedance probability decreases with an increase in the structure's height and SSI consideration adapts to lower exceedance probability for the studied structures.
- 7. Finally, it can be stated that intermediate moment-resisting steel frame structures designed according to ASCE7-16 consideration have an acceptable seismic performance against far-field records in a way that their exceedance probabilities reaching the LS and CP performance levels are less than 0.45 and 0.03, respectively.

#### References

1. Federal Emergency Management Agency “Quantification of building seismic performance factors”, US Department of Homeland Security, FEMA (2009).
2. Allotey, N.K., *Nonlinear Soil-Structure Interaction in Performance-Based Design*, ProQuest (2008).
3. SAC Joint Venture “Recommended seismic design criteria for new steel moment-frame buildings”, Washington, DC, USA: Federal Emergency Management Agency, **350** (2000).
4. FEMA 356, *Pre-standard and Commentary for the Seismic Rehabilitation of Buildings* (2000).
5. Vamvatsikos, D. and Cornell, C.A. “Incremental dynamic analysis”, *Eart. Eng. and Str. Dyn.*, **31**(3), pp. 491–514 (2002).
6. Suyehiro, K. “Engineering seismology: Notes on American lectures”, *Proc. Amer. Soc. Civil Engin.*, **58**(4), pp. 1–110 (1932).
7. Kanai, K., *Engineering seismology*, Tokyo: University of Tokyo Press (1983).
8. Kanai, K. “A study of strong earthquake motions”, Bulletin of the Earthquake Research Institute, University of Tokyo, **36**(3), pp. 295–310 (1958).
9. Biot, M.A. “Theory of propagation of elastic waves in a fluid-saturated porous solid. II. Higher frequency range”, *The J. of the Acou. Soc. of America*, **28**(2), pp. 179–191 (1956).
10. Gazetas, G. and Mylonakis, G. “Seismic soil-structure interaction: new evidence and emerging issues”, *Geo. Spe. Pub.*, **75**(2), pp. 1119–1174 (1998).
11. Gazetas, G. and Apostolou, M. “March. nonlinear soil-structure interaction: foundation uplifting and soil yielding”, In *Pro. Third UJNR Workshop on Soil-Structure Interaction*, pp. 29–30 (2004).

12. Radkia, S., Rahnavard, R., Tuwair, H., et al. "Investigating the effects of seismic isolators on steel asymmetric structures considering soil-structure interaction", *In Str.*, **27**, pp. 1029–1040, Elsevier (2020).
13. Liu, S., Li, P., Zhang, W., et al. "Experimental study and numerical simulation on dynamic soil-structure interaction under earthquake excitations", *Soil Dyn. and Eart. Eng.*, **138**, p. 106333 (2020).
14. Mashhadi, S., Asadi, A., Homaei, F., et al. "Seismic response of mid-rise steel MRFs: the role of geometrical irregularity, frequency components of near-fault records, and soil-structure interaction", *Bul. of Eart. Eng.*, pp. 1–25 (2021).
15. Vaseghiamiri, S., Mahsuli, M., Ghannad, M.A., et al. "Probabilistic approach to account for soil-structure interaction in seismic design of building structures", *J. of Str. Eng.*, **146**(9), p. 04020184 (2020).
16. Arboleda-Monsalve, L.G., Mercado, J.A., Terzic, V., et al. "Soil-structure interaction effects on seismic performance and earthquake-induced losses in tall buildings", *J. of Geo. and Geoenv. Eng.*, **146**(5), p. 04020028 (2020).
17. Bai, J., Chen, H., Jia, J., et al. "New lateral load distribution pattern for seismic design of deteriorating shear buildings considering soil-structure interaction", *Soil Dyn. and Eart. Eng.*, **139**, p. 106344 (2020).
18. Kennedy, R.P., Cornell, C.A., Campbell, R.D., et al. "Probabilistic seismic safety study of an existing nuclear power plant", *Nuc. Eng. and Des.*, **59**(2), pp. 315–338 (1980).
19. Kircher, C.A. and Martin, W. "Development of fragility curve for estimating of earthquake damage", *In the Work Shop on Continuing Action to Reduce losses from Earthquake*, Washington, DC: US Geological Survey (1993).
20. Anagnos, T., Rojahn, C., and Kiremidjian, A.S. "Building fragility relationships for California", *In Proceedings of the Fifth US National Conference on Earthquake Engineering*, pp. 389–396 (1994).
21. Biglari, M., Formisano, A., and Hashemi, B.H. "Empirical fragility curves of engineered steel and RC residential buildings after Mw 7.3 2017 Sarpol-e-zahab earthquake", *Bul. of Eart. Eng.*, **19**(6), pp. 2671–2689 (2021).
22. Mohebi, B., Yazdanpanah, O., Kazemi, F., et al. "Seismic damage diagnosis in adjacent steel and RC MRFs considering pounding effects through improved wavelet-based damage-sensitive feature", *J. of Bui. Eng.*, **33**, p. 101847 (2021).
23. Taiyari, F., Formisano, A., and Mazzolani, F.M. "Seismic behaviour assessment of steel moment resisting frames under near-field earthquakes", *Int. J. of Ste. Str.*, **19**(5), pp. 1421–1430 (2019).
24. Yazdanpanah, O., Formisano, A., Chang, M., et al. "Fragility curves for seismic damage assessment in regular and irregular MRFs using improved wavelet-based damage index", *Measurement*, **182**, p. 109558 (2021).
25. Karafagka, S., Fotopoulou, S., and Pitilakis, D. "Fragility curves of non-ductile RC frame buildings on saturated soils including liquefaction effects and soil-structure interaction", *Bul. of Eart. Eng.*, pp. 1–26 (2021).
26. Petridis, C. and Pitilakis, D. "Fragility curve modifiers for reinforced concrete dual buildings, including non-linear site effects and soil-structure interaction", *Eart. Spe.*, **36**(4), pp. 1930–1951 (2020).
27. Forcellini, D. "Analytical fragility curves of shallow-founded structures subjected to Soil-Structure Interaction (SSI) effects", *Soil Dyn. and Eart. Eng.*, **141**, p. 106487 (2021).
28. Hamidia, M., Shokrollahi, N., and Nasrolahi, M. "Soil-structure interaction effects on the seismic collapse capacity of steel moment-resisting frame buildings", *In Str.*, **32**, pp. 1331–1345, Elsevier (2021).
29. Nasab, M.S.E., Chun, S., and Kim, J. "Soil-structure interaction effect on seismic retrofit of a soft first-story structure", *In Str.*, **32**, pp. 1553–1564, Elsevier (2021).
30. Shahbazi, S., Khatibinia, M., Mansouri, I., et al. "Seismic evaluation of special steel moment frames subjected to near-field earthquakes with forward directivity by considering soil-structure interaction effects", *Sci. Ira.*, **27**(5), pp. 2264–2282 (2020).
31. Güneş, N. and Ulucan, Z.Ç. "Collapse probability of code-based design of a seismically isolated reinforced concrete building", *In Str.*, **33**, pp. 2402–2412, Elsevier (2021).
32. Güneş, N. "Comparison of monotonic and cyclic pushover analyses for the near-collapse point on a mid-rise reinforced concrete framed building", *Eart. and Str.*, **19**(3), pp. 189–196 (2020).
33. Csi, C. "Analysis reference manual for SAP2000, ETABS, and SAFE", *Computers and Structures*, Berkeley, California, USA (2016).
34. American Society of Civil Engineers "Minimum design loads and associated criteria for buildings and other structures" (2017).
35. Bazzurro, P. and Cornell, C.A. "Seismic hazard analysis of nonlinear structures. I: Methodology", *J. of Str. Eng.*, **120**(11), pp. 33200–3344 (1994).
36. Foutch, D.A. and Yun, S.Y. "Modeling of steel moment frames for seismic loads", *J. of Con. Ste. Res.*, **58**(5-8), pp. 529–564 (2002).
37. Ramanathan, K.N., *Next Generation Seismic Fragility Curves for California Bridges Incorporating the Evolution in Seismic Design Philosophy*, Georgia Institute of Technology (2012).
38. Baker, J.W. and Allin Cornell, C. "A vector-valued ground motion intensity measure consisting of spectral acceleration and epsilon", *Eart. Eng. and Str. Dyn.*, **34**(10), pp. 1193–1217 (2005).
39. Gcr, N., *Soil-Structure Interaction for Building Structures*, National Institute of Standards and Technology (NEHRP) (2012).

40. Givens, M.J., *Dynamic Soil-Structure Interaction of Instrumented Buildings and Test Structures*, University of California, Los Angeles (2013).
41. Kausel, E. "Early history of soil-structure interaction", *Soil Dyn. and Earth Eng.*, **30**(9), pp. 822–832 (2010).
42. Gajan, S., Raychowdhury, P., Hutchinson, T.C., et al. "Application and validation of practical tools for nonlinear soil-foundation interaction analysis", *Earth. Spe.*, **26**(1), pp. 111–129 (2010).
43. Raychowdhury, P., *Nonlinear Winkler-Based Shallow Foundation Model for Performance Assessment of Seismically Loaded Structures*, University of California, San Diego (2008).
44. Allotey, N. and El Naggar, M.H. "An investigation into the Winkler modeling of the cyclic response of rigid footings", *Soil Dyn. and Earth Eng.*, **28**(1), pp. 44–57 (2008).
45. Harden, C.W., *Numerical Modeling of the Nonlinear Cyclic Response of Shallow Foundations*, Pacific Earthquake Engineering Research Center (2005).
46. Mazzoni, S., McKenna, F., Scott, M.H., et al. *OpenSees Command Language Manual*, Pacific Earthquake Engineering Research Center, **264**, pp. 137–158 (2006).
47. Foutch, D.A. and Yun, S.Y. "Modeling of steel moment frames for seismic loads", *J. of Con. Ste. Res.*, **58**(5–8), pp. 529–564 (2002).
48. Rajeev, P. and Tesfamariam, S. "Seismic fragilities of non-ductile reinforced concrete frames with consideration of soil structure interaction", *Soil Dyn. and Earth Eng.*, **40**, pp. 78–86 (2012).
49. Dutta, S.C. and Roy, R. "A critical review on idealization and modeling for interaction among soil-foundation-structure system", *Comp. and Str.*, **80**(20–21), pp. 1579–1594 (2002).
50. Mehdizadeh, K. and Karamodin, A. "Probabilistic assessment of steel moment frames incremental collapse (ordinary, intermediate and special) under earthquake", *J. of Str. and Con. Eng.*, **4**(3), pp. 129–147 (2017).
51. Suita, K., Yamada, S., Tada, M., et al. "Collapse experiment on 4-story steel moment frame: Part 2 detail of collapse behavior", In *Proceedings of the 14th World Conference on Earthquake Engineering*, Beijing, China, **11** (2008).
52. Lignos, D.G., Hikino, T., Matsuoka, Y., et al. "Collapse assessment of steel moment frames based on E-Defense full-scale shake table collapse tests", *J. of Str. Eng.*, **139**(1), pp. 120–132 (2013).
53. American Society of Civil Engineers. "Seismic Evaluation and Retrofit of Existing Buildings ASCE/SEI 41-13" (2014).
54. Haselton, C.B., Liel, A.B., Deierlein, G.G., et al. "Seismic collapse safety of reinforced concrete buildings. I: Assessment of ductile moment frames", *J. of Str. Eng.*, **137**(4), pp. 481–491 (2011).
55. Baker, J.W. "Efficient analytical fragility function fitting using dynamic structural analysis", *Earth. Spe.*, **31**(1), pp. 579–599 (2015).

## Biographies

**Mahyar Sabouniaghdam** received his BSc (2015) in Civil Engineering from Islamic Azad University at South Tehran branch and MSc (2019) in Earthquake Engineering from Iran University of Science and Technology, Tehran, Iran. His research interests include probabilistic collapse assessment and soil-structure interaction.

**Esmaeil Mohammadi Dehcheshmeh** is a PhD Candidate in Civil Engineering and a Research Assistant at Iran University of Science and Technology, Tehran, Iran. He received his BSc (2013) from Tabriz University and MSc (2016) from Iran University of Science and Technology. His research interests include self-centering structures, progressive collapse, soil-structure interaction, reliability based design optimization, and machine learning.

**Pouria Safari** is a Research Assistant at the Structural Engineering Group of the School of Civil Engineering at Iran University of Science and Technology, Tehran, Iran. He received his BSc (2016) in Civil Engineering from Sharif University of Technology and MSc (2018) in Structural Engineering from Iran University of Science and Technology. His research interests include structural failure analysis, computational simulation, and finite element analysis.

**Vahid Broujerdiyan** is an Assistant Professor of Structural Engineering and the Head of Structural Engineering Group at the School of Civil Engineering at Iran University of Science and Technology. He received his BSc (2002), MSc (2004), and PhD (2010) in Structural Engineering from Sharif University of Technology, Tehran, Iran. His research interests include analytical and numerical study of nonlinear behaviour of materials and structures, design and analysis of wind and earthquake resistant structures, and design and analysis of structures against abnormal conditions (impact, blast, and fire).